ICAS-88-3.7.3

TURBULENT BOUNDARY LAYER MANIPULATION IN ZERO PRESSURE GRADIENT

E. Coustols and J. Cousteix
O.N.E.R.A./C.E.R.T.
Aerothermodynamics Department
2, avenue Edouard Belin
31055 Toulouse Cedex
France

Abstract

Interest in reducing the drag of aerodynamic surfaces has led to the control of the turbulent skin friction evolution. The problem of explaining cause and effect relationships is surely one of the most challenging tasks ; this has been undertaken with two drad-reducing methods : thin flat plate or aerofoil section devices embedded within the boundary layer and surface modification in the form of longitudinal ribs : "riblet" surfaces. This paper presents detailed anemometry measurements (straight and cross hot-wire surveys, spectral analysis...) wall shear stress measurements and pressure fluctuations spectra for these two passive approaches. So, detailed experimental information is then available ; it provides us with a good description of mechanisms leading to such a turbulent drag reduction.

I. Introduction

The prospect of significant saving in fuel and improved performance has stimulated interest in devices for manipulating the structure of the boundary layers which develop on wing, drift, nacelle, fuselage... with the objective of reducing skin-friction. Let us recall that the two main sources of drag are the friction drag due to boundary layers and the lift induced drag evidenced essentially by marginal wingtip vortices. They respectively account for 48% and 37% of the total drag of a modern subsonic transport aircraft[1]. According to the importance of the latter, one could think there exists a tremendous potential for drag reduction. But, one has to be aware that this peculiar drag is in proportion to the square of the lift coefficient which has to be rather high ; so, real opportunities for such a drag decrease are, in fact, confined enough. However, let us point out that some Airbus-type transport aircrafts are flying with wing tip fences.

As it has been said before, the greatest part of the total drag rests with the friction drag. It is, most of the time, in this field that the impetus for drag reduction research has been the most complete. Even a very small percentage reduction in drag would provide saving in cost of astronomical proportions.

Considering a transport aircraft, one way of reducing the friction drag is to find a way of stretching out the laminar flow over as long a path of boundary layer as possible. This is done by controlling the stability properties of the laminar boundary layer with an active device (wall suction - "Hybrid Laminar Flow Control"), or a passive device (favourable pressure distributions - "Natural Laminar Flow"), or a combination of the two. Maintaining laminar flow seems to be a realistic approach when the Reynolds number is relatively low, which is the case of wings, nacelles, drifts or empennages. For fuselages, though, where the Reynolds number is higher, it is much more difficult to maintain the laminar flow. The interest has, then, led to the control of the structure of turbulent boundary layers. That structure is related to a cycle of consistent individual events featuring ejections near the wall, entrainment of large scale structures, penetration of irrotational fluid into the boundary layer.One must say that, during the last decade, the study of boundary layer flow phenomena has been concentrated upon the so-called "coherent structures". A great effort has been devoted in order to detect and analyze those structures, though all the investigators are not completely in agreement. Thus, new drag reduction methods have been largely stimulated by the recognition of identifiable flow patterns, providing mechanisms for turbulence production, for instance. Whatever methods for turbulent boundary layer drag reduction are considered, it seems rather evident that their action will be closely involved with a modification of the turbulence production process.

During the last ten years or so, numerous experiments have been performed in an attempt to manipulate turbulent boundary layers in order to produce nett performance benefits in terms of nett drag reductions. Active and passive methods have been considered ; articles published recently by Bushnell[2] and Thomas[3] catalogue in detail the processes studied until now. Wilkinson et al. even suggest "the approaches which work, the approaches which may work, the approaches which evidently do not work"[4].

Among all the existing passive methods (which work), two of them have been considered in detail for about three years now, at ONERA/CERT :

- insertion of devices within the external part of the boundary layer : external manipulators or devices[5],[6] ;
- alteration of the wall geometry with small streamwise surface grooves : internal manipulators or devices[6],[7].

The ONERA/CERT effort in turbulent drag reduction is still on going and involves research in both theoretical studies as well as experimental ones (experiments conducted in subsonic flows, in transonic flows and on slender bodies). The present paper summarizes the status of this research carried out in low speed wind-tunnel. The objective is to explore the effects of the external as well as internal manipulators on the mean and fluctuating quantities of a 2D-turbulent boundary layer, and to give an estimate of drag reduction performances of such passive devices.

II. Experimental apparatus for low speed laboratory experiments

Experiments, involving both manipulators, have been performed in the same wind-tunnel at low subsonic free-stream speeds and with nominally 2D flows developing on the lower floor of the test section. The cross-section is rectangular : 30 cm high, 40 cm wide and approximately 120 cm long. The upper and lower walls of the test section diverge slightly to achieve practically a zero-pressure gradient flow. Static pressure probe measurements made along the centerline of the test section indicate a slight favourable pressure gradient ($1/Ue \cdot dUe/dx = 0.6\%$) over the whole length of the test section. Considering the integral momentum equation, the contribution of this resulting external velocity gradient is negligible in front of the variation of momentum thickness.

The turbulence level in the external flow is roughly constant and of the order of 0.25% for outer flow velocity range : 18 - 36 ms^{-1} ; at lower free-stream velocities, this turbulence level increases slightly to reach 0.4% at about 14 ms^{-1}. Preliminary surveys were made in the potential flow through a four-wire probe, developed at ONERA/CERT by Pailhas et al.[8] ; they allowed to control the 2-Dimensionality of the flow. For a given free-stream velocity (24 ms^{-1}), the modulus of the cross flow does not exceed 0.15 ms^{-1} over a transverse distance close to 250 mm ; consequently, the angle between the streamwise and cross flow components of the external velocity profile is less than 0.5°.

A cylindrical wire is fixed to the lower wall of the collector, about 250 mm ahead of the test section inlet, so as to set off the transition for the considered free-stream velocities and thicken the parietal boundary layer. Hot wire surveys have been performed for different external velocities, U_∞ , at an abscissa located about 1 m downstream of the trip. These anemometry measurements have provided us with the evolutions of the momentum thickness, θ , and the skin friction coefficient, Cf, versus U_∞ ; specifically, this curve $\theta(U_\infty)$ will be used as reference for the estimate of the drag coefficient. When plotting $U_\infty^{1/6}\ \theta$ versus the external velocoity, for $14 \leq U_\infty \leq 36$ ms^{-1}, one gets a constant value ; that means that the virtual origin of the turbulent boundary layer is fixed whatever the value of U_∞ is.

External manipulators

The manipulators embedded within the external part of the boundary layer are located at about 0.5 m from the tripping wire, at a distance where the turbulent boundary layer approaching the devices goes back to an equilibrium state. For this set of laboratory experiments, two different kinds of manipulators have been considered :

- devices are thin clinker steel flat plates. In that case, different thicknesses (t) as well as chord lengths (c) are available : t = 0.08 - 0.20 mm; c = 12.7 - 25 mm.
- devices made from carbon fiber, having an aerofoil section NACA 0009. For this specific manipulator, a single chord length is available c = 20 mm. These aerofoil-shaped devices are required if one wants to bring this drag reduction system at higher speeds, closer to flight tests, because of their stiffness.

In both cases, the manipulator devices are mounted between two supports, each of them having a transverse degree of freedom. This way, it is possible to apply a tension to the devices during the tests in order to eliminate any vibration they may have ; this is particularly the case for the thin clinker steel manipulators.

Internal manipulators

The boundary layer developing along the lower wall of the test section is manipulated by varying the geometry of the wall. The floor is equipped with four identical removable plates, the length of which is 0.32 m ; this set-up allows to replace very easily smooth plates by "riblet" ones. Two manipulated lengths have then been tested : 0.32 m and 0.64 m ; then, the leading edge of the grooved plates is either distant from 0.67 m or 0.35 m to the tripping wire. Let us add that the experimental set-up allows to test the "riblet" models with either their bases (configuration B) or their tops (configuration T) aligned flush with the upstream and downstream adjacent smooth walls.

The considered models allow to evaluate the effect of rib spacing, rib height and rib cross section shape. Three machined aluminium surfaces ($s = h = 0.25$ mm, $s = 2h = 0.50$ mm, $s = 3h = 0.60$ mm) as well as two models form thin vinyl sheet having an adhesive backing ($s = h = 0.152$ mm - from 3M Company - and $s = 0.46$ mm $\#$ 3.5 h) have been tested, where s and h denote respectively the spacing and the height of the "riblet". The last model ($s \# 3.5\ h$) has been selected to evaluate the sensitivity of this drag reducing process to peak and valley curvature whereas the first four "riblet" geometries consisted of symmetric V-grooves with sharp peaks and valleys.

III. External manipulators

Thin manipulators, having either a rectangular or an aerofoil section, settled within the external part of a turbulent boundary layer have been extensively investigated experimentally this last couple of decades as regards to their potential to provide with turbulent drag reduction but also to obtain knowledge of turbulent boundary layer structures. They are commonly referred to as "LEBU" (Large Eddy Break-Up devices), "BLADE" (Boundary Layer Alteration DEvices), "OLD" (Outer Layer Devices), ribbons, turbulence manipulators... Considerable effort, for most of it in the United States and in Europe, has been expended in an attempt to define optimum parameters (geometrical device configuration) where "optimum" has been taken to mean either greatest averaged skin friction reduction over the considered test section length or greatest nett drag reduction at the furthest downstream location. Though there is some disagreement concerning the magnitude of reduction, most of the research groups usually quotes figures of the order of 6 - 8% of maximum nett drag reduction[9],[10],[11],[12],[13] and [14]. These substantial reductions could be achieved with very thin plates carefully machined, set-up and tensioned to avoid any vibration. All these precautions could explain the noticeable variability of results from some laboratory to another. Besides that, the huge variations between the different results could come from the low-chord Reynolds numbers (Rec < 100 000)

of all tests to date[11].

In any practical applications, such thin plate manipulators will be replaced by stronger, self-supporting, aerofoil section devices. Low speed laboratory experiments have shown that these devices could produce up to 7% of nett drag reduction[11]. Let us add that Anders[15] published rather recently a summary of all the drag reduction data obtained, to his knowledge, through outer layer devices. (The reader can find there a non-exhaustive list of most of the papers published in this drag reduction field).

It has been well established, through careful low speed experiments, that external manipulators can provide with nett drag reduction in turbulent boundary layers. However, the physical changes, produced by these devices, have been currently a topic of research. If one wants to extrapolate performance in aircraft and/or other technological applications, one needs to elucidate the mechanisms which are responsible for the reduced skin-friction.

So, at ONERA/CERT, experiments have been conducted in a way to look at device performance in terms of drag reduction and to try to understand the process which alters the development of the turbulent boundary after such a manipulation. It was then felt that detailed hot-wire and wall shear stress measurements, especially in the immediate vicinity of either thin plates or aerofoil section devices would be very helpful.

Rectangular section devices (clinker steel flat plates).

At the location selected for both single- and tandem-type configurations, the main characteristics of the undisturbed boundary layer are : external free-stream velocity (U_∞) close to 24 ms^{-1}, boundary layer thickness δ_0 # 17 mm and Reynolds number based on the momentum thickness R_θ # 2400.

The first low speed experiments have been undertaken with a single device, the chord length of which was fixed and equal to 12.7 mm. These experiments have been performed in a way to determine the thickness and position of the small plate within the boundary layer that would produce the greatest nett drag reduction. This parametric study has resulted in the following geometry configuration : $c/\delta_0 = 0.75$, $t/\delta_0 = 0.007$, $h/\delta_0 = 0.3$. Figure 1 illustrates the global effect the insertion of such a device has on the mean characteristics of the boundary layer. It is very tempting to interpret the momentum thickness variation by relating θ to some drag coefficient. Though this analysis is too crude near the manipulator trailing edge since it implicitely assumes that the pressure is uniform throughout the flow, we can nontheless say that the increase in θ at the device location is due to its own drag and that the lower slope of the θ-curve is related to a decrease in the skin-friction coefficient. At the further downstream station, along the available test section length, one can neglect any manipulator induced pressure variations. So the comparison of momentum thickness with and without manipulator at that location allows us to judge of an increase or decrease in the drag coefficient. For that specific geometry configuration, the nett drag reduction reached over 50 δ_0 length of manipulated boundary layer is of the order of 4%[5].

The skin friction coefficient, Cf, was measured directly, downstream of the manipulator performance, using several hot-element skin friction gauges developed at ONERA/CERT by Houdeville et al.[16] since indirect methods , such as Clauser technique, are not valid anymore when the boundary layer is caution to manipulation. The results are given on figure 2 where the quantity Cf/Cf_{ref} represents the reduction in the local skin friction coefficient ; 10% of maximum local reduction is recorded at about X/δ_0 close to 10 where X = 0 refers to the trailing edge of the device. The resultant force of the integral of Cf is reduced which agrees with the decrease in the slope of the θ-curve.

Then, further studies have been carried out with a tandem plate-type configuration. Using the same parametric investigation as for a single device, that leads us to the following geometry characteristics : $t/\delta_0 = 0.007$, $c/\delta_0 = 1.2$, $s/\delta_0 = 6$, $h_1/\delta_0 = h_2/\delta_0 = 0.35$ where h_1 and h_2 denote respectively the heights of the upstream and downstream thin plates and s the spacing between the two leading edges. By plotting θ versus the streamwise abscissa, the available development length (which is in that case close to 40 δ_0) is not long enough to get any overall benefit (figure 1). However, the local Cf reduction is greater (maximum of the order of 20%) in the tandem-type configuration than in the single-type configuration (figure 2) ; this observation illustrates the beneficial effect of the two devices though the drag of the manipulator itself is increased (figure 1). As the skin-friction recovery is slower in that configuration, one might think that a greater manipulated length would have provided with nett reduction since the mean local Cf reduction almost balances the manipulator drag over 40 δ_0.

It is interesting to notice that a small nett drag reduction has been achieved with thin flat plate device over such a short distance. This might come from the rather small value of t/δ_0 , compared to the ones generally mentioned throughout the literature. Detailed anemometry measurements performed for the two configurations described above can be found in [5] and [6].

Aerofoil section devices (NACA 0009 devices)

For higher speeds tests and, consequently for practical applications such thin plate manipulators will have necessarily to be replaced by devices having a greater structural rigidity such as aerofoil shaped devices. But, at first, low speed laboratory experiments are needed in order to check, for instance, if similar skin friction reductions can be achieved with these latter, if they behave in the same way...

As the geometry of the device is fixed, the influence of the manipulator position within the boundary layer as well as the effect of the chord Reynolds number have been examined. Three external free-stream velocities have been considered U_∞ # 16, 24 and 32 ms^{-1} to which correspond Rc (chord Reynolds number) # 21 100, 31 700 and 42 200. At the leading edge of the single, or upstream, device the natural boundary layer thickness is close to 17 - 18 mm and the momentum Reynolds numbers are respectively about 1 500, 2 300 and 2 900.

Skin friction reduction :

As for the devices having a rectangular section, the skin friction coefficient has been measured directly with six hot-element skin-friction gauges and a servo-controlled floating element drag balance set up at Laval University, Quebec[17]. Cf measurements have been performed for each of the free-stream velocity ; results are only presented for $U_\infty \# 32\ ms^{-1}$, i.e. Rc # 42 200 (fig. 3, 4 and 5). Let us add that the level of maximum local reduction is not strongly dependant of the value of the chord Reynolds number, at least for the explored range which corresponds to relatively low values of Rc.

For a single device (fig. 3), maximum reduction of approximately 20% has been recorded for $h/\delta_0 \# 0.24$. Measurements have shown, the closer the manipulator is to the wall, the greater the maximum of local reduction is. The relaxation of the skin-friction coefficient depends upon the manipulator position within the boundary layer : it seems to be slower when h is high but, in any case, it is not yet terminated over the manipulated length close to 50 δ_0.

For different tandem spacings, $s/\delta_0 \# 6$ and 12, greater local reductions, close to 30%, have been obtained at $h/\delta_0 \# 0.24$ (fig. 4 and 5). As the height of the manipulator increases, the abscissa of maximum local reduction moves downstream ; some experimental studies, based on flow visualisations, have revealed that this abscissa roughly corresponds to the point where the device wake reaches the wall. For these considered spacings, the relaxation of the skin-friction coefficient is far from being terminated, since about 10% of reduction is recorded at a distance close to 50 δ_0 from the trailing edge of the upstream device.

For s = 6 δ_0 (fig. 4), the first gauge is just upstream to the leading edge of the downstream device ; results indicate a lower value of Cf since the device inevitably induces a pressure variation in its immediate vicinity and the flow is decelerating just ahead of the second aerofoil-shaped device. However for s = 12 δ_0 (fig. 5), the same Cf value is recorded at the same location. Furthermore, in that case, the second gauge has been judiciously set to match the downstream device location ; important increases in the skin friction coefficient have been obtained, especially when the manipulator is close to the wall, because of the acceleration of the flow below it. Figures 4 and 5 show clearly the beneficial effect of tandem configurations as regards to greater local Cf reduction and slower recovery.

Let us point out the good agreement between hot film gauges and drag balance measurements since the guessed evolution of the Cf coefficient, given by the smoothed curve, goes pretty well through the experimental data points. As regards to skin friction reduction, a lot of similarities exist between devices having either a rectangular or an aerofoil section. The above results have been recently compared by Lemay et al. to those obtained with thin ribbons at CEAT Poitiers and thick ones at Cambridge University[18]. Since the devices are profiled, the authors considered they have both some of the thin and thick device characteristics.

Detailed anemometry measurements for a given configuration :

The effeciency of such devices, in terms of drag reduction performances, has been checked by looking at the momentum thickness, θ, obtained through hot-wire surveys at the furthest downstream location[6]. Results of this study have shown that whatever configuration is considered, there is no nett drag reduction. One has to be aware that for the tandem spacing $s/\delta_0 = 12$, the available manipulated length downstream of the manipulator is rather short (close to 37 δ_0). However, it is in that case that the drag increase is the smallest, for an height close to 0.3 δ_0.

The effect of chord Reynolds number has also been carefully examined[6] ; it appears that, for tamdem-type configurations, this effect seems to be benefit for drag-reducing process since increasing Rc gives smaller drag increase.

Then, it was decided to carry out a detailed analysis for a specific configuration which could produce a nett drag reduction if, for instance, the manipulated length be longer. Numerous hot-wire measurements (straight and crossed wires) as well as spectral analysis have been performed in the following configuration : $c/\delta_0 \# 1.2$, $s/\delta_0 \# 12$, $h/\delta_0 \# 0.3$, $\delta_0 \# 17$ mm and Rc # 42 200.

- Characteristics of the mean flow :

Figure 6 illustrates the evolution of the momentum thickness, θ, behind both upstream and downstream devices. Let us notice that Xu = 0 (respectively Xd = 0) refers to the trailing edge of the upstream (respectively downstream) device.

In the immediate vicinity of the devices trailing edges, the momentum thickness is decreasing. This has to be associated to the device wake since the aerofoil-shaped devices induce an important pressure variation, in fact a negative pressure gradient in the downstream vicinity of their trailing edges. This could not be observed with thin flat plates because the modifications on the pressure field were weaker ; the device thickness and consequently the wake thickness is not large enough to produce such an effect.

At about two to three chord lengths behind each device, θ begins to increase. Around this location, the over thickening is greater for the downstream device than for the upstream one because of the device drag itself. One can also observe that the slope of the θ-curve is smaller for the manipulated boundary layer than for the non-manipulated boundary layer : the difference is close to 12% which is in good agreement with the measured skin-friction coefficient evolution.

For this specific configuration, the drag increase is close to 4 - 5% ; we can however quote that the drag penalty of the manipulator is almost balanced over 37 δ_0 of manipulated length. The results obtained are quite comparable to those described in a preceding paragraph with small flat plates which is very confident for higher speed tests.

Hot-wire surveys have been made at 7 stations between the two devices and 10 stations behind the

downstream one. The development of the wake of the manipulator around h = 5.1 mm from the wall (h/δ_0 = 0.3) is clearly visible on mean velocity profiles[6]. The velocity deficit pocket is gradually taken up as the manipulator wake mixes to the whole flow. The region where the wake is obviously apparent within the boundary layer extends over about 5 δ_0 from the trailing edge of each device.

- Reynolds Stress profiles :

In fact, the analysis of the three components of the Reynolds Stress tensor have revealed quite a lot of details concerning the interaction : manipulator wake-turbulent boundary layer. The effect of the manipulators is, indeed, more pronounced when the r.m.s. values are compared.

This iso-streamwise velocity fluctuations are plotted behind the upstream (resp. downstream) device in a (Y/δ_0 , Xu/δ_0) (resp. (Y/δ_0 , Xd/δ_0)) plane on figures 7b et 7c ; they are compared to those obtained without manipulators (fig. 7a). Close to the upstream device, one can observe a surplus of turbulence intensity ; this latter approaches 13% around h = 5.1 mm which is about twice the turbulence level of the undisturbed boundary layer. This peak gradually decreases up to X/δ_0 = 0.6, then the turbulence intensity becomes smaller than without the device, especially below y = h. The r.m.s. value reaches a maximum reduction of about 30% at y/δ_0 = 0.24 and Xu/δ_0 = 2.4. So, the turbulence generated by the manipulator, which, at first, simply superimposes upon the pre-existing turbulence, tends to impose its own structure since it has a much smaller scale and, consequently its rate of decay is greater. Same kinds of observations can be made downstream of the second device (fig. 7c) .The peak of turbulence intensity is weaker but is still superimposed to the turbulence already altered by the upstream device. The significant reduction is even greater (maximum close to 36% at y/δ_0 = 0.28 and Xd/δ_0 = 1.18).

Let us point out that the normal to the wall turbulence intensity profiles are a little bit more affected than the streamwise ones ; the surplus of turbulence subsists on a longer downstream distance and the decrease in turbulence level is less important compared to the u'-profiles[6].

The iso-shear stress contours are plotted on figures 8b and 8c for the manipulated boundary layer. The manipulator effect is more spectacular on turbulent shear stress profiles. The correlation is immediately suppressed over a greater vertical extent than the streamwise and vertical intensity profiles. The friction profiles exhibit a very important reduction below the wake of the manipulator. For $0.12 \leq Xu/\delta_0 \leq 0.72$ negative values of $-\overline{u'v'}$ are recorded. Thus, a pocket of negative or near-zero production is detected since the sign reversals of the Reynolds stress and the mean shear ($\partial U/\partial y$) do not exactly coincide. As the wake widens gradually and decays downstream, this important shear stress reduction decreases.

At further locations, beyond Xd/δ_0 # 30 , an excess of production can be observed on the $\overline{u'v'}$ components of the Reynolds tensor ; moreover, let us point out that small overshoots have also been observed on the v'-profiles but not on the u'-profiles. This observation might suggest that the turbulent profiles did not go back to an equilibrium state, yet, at downstream abscissa up to 35 δ_0 . There must be a redistribution of turbulent kinetic energy as it was quoted by Lemay et al.[18] and pointed out by Guezennec et al.[19] in their experiments.

- Spectral Analysis :

... $\overline{u'^2}$ and $\overline{v'^2}$ spectra :

The spectral analysis, developed at ONERA/CERT by Pailhas[20], is divided into two parts : a low frequency zone (20 Hz - 500 Hz) and high frequency one (500 Hz - 20 KHz). The final spectrum results from an average of 50 intermediary spectra for the high frequency part and 100 intermediary spectra for the low frequency range.

Using a miniature X-wire probe (distance between the wires : 0.6 mm, 5 µm diameter wire) streamwise (fig. 9) and normal to the wall (fig. 10) velocity spectra have been performed at several abscissa behind the upstream aerofoil shaped device. Data are presented for only two streamwise locations Xu/δ_0 = 0.06 and 4.71 but at different heights within the boundary layer ; heights centered around the device location. The dashed lines refer to the spectra obtained for the non-manipulated boundary layer. Spectra are presented in a log-log representation where F corresponds to the energy density associated with the wave number $k = 2\pi f/U$ (f is the physical frequency and U the mean local streamwise velocity at the given height). The function F(k) has been normalized in such a way that its integral is equal to 1.

The effect of manipulation on $\overline{u'^2}$ spectra is illustrated on figure 9. At Xu/δ_0 = 0.06, the manipulator wake is clearly visible at y = 5 mm with a characteristic double mid-range bump in the spectrum. At this same altitude, one can observe an excess at high wave numbers which reveals a production of new energetic small scales and a deficit at low wave number which leads to the suppression of the large scale structures. These deficit and excess persist for other streamwise abscissa and spread to the neighbouring altitudes. At Xu/δ_0 = 4.71, the inertial region properties (- 5/3 slope for the non-manipulated spectra) are not any longer valid. Let us point out that, at the closest abscissa to the trailing edge of the device, the observed peak on the u'^2-spectra corresponds, of course, to the same frequency - related to the time scale of the eddies in the near wake rather than any vibrational effect - but different wave numbers k since the mean local streamwise velocity is varying within the height y.

For the $\overline{v'^2}$-spectra, one can note that the double structure is not as pronounced as it is the case for $\overline{u'^2}$-spectra at Xu/δ_0 = 0.06 (fig. 10). Nevertheless, whatever streamwise abscissa is considered, it appears that the deficit at low wave numbers seems greater than for the streamwise velocity spectra. On the other hand, the excess of energy density at high wave numbers seems to be of the same order of magnitude and even a little bit smaller.

This analysis shows up clearly the damping of the large scale structures and the production of new energetic small scales. This result is consistent with those obtained by Lemay et al.[18] and

Savill[21].

... $\overline{p'^2}$ spectra :

Besides the drag reduction field, there is quite a large number of "intriguing possible applications for large-eddy breakup devices" as quoted by Wilkinson et al.[4]. One of them consists to look at the reduction (if there is any) of pressure fluctuations downstream of the external manipulator. This might be interesting for hydrodynamic vehicles.

So, we used the experimental set-up developed at ONERA/CERT for the study of correlation pressure - velocity fluctuations within a transitional region[22] ; small microphones are mounted flush with the smooth wall. Two locations have been selected : $Xd/\delta_0 = 0.8$ and 5.5. This latter corresponds approximately to the maximum of local skin-friction reduction. The range of explored frequencies is : 250 Hz - 25 KHz. Four positions of the tandem type configuration have been considered : h = 25, 12, 6 and 3 mm that is to say $h/\delta_0 = 1.5$, 0.71, 0.35 and 0.18. The $\overline{p'^2}$ spectra are plotted on figure 11-a for $Xd/\delta_0 = 0.8$ and on figure 11-b for $Xd/\delta_0 = 5.5$. When the manipulator is set outside the boundary layer, one can observe a peak which superimposes to the initial undisturbed spectrum, corresponding to a frequency close to 8 500 Hz ; this peak disappears when the device is dived within the turbulent boundary layer. Let us point out that this peculiar frequency decreases when the external free-stream velocity diminishes. The frequency is associated to the new eddies generated in the manipulator wake since , by scaling it with the wake thickness, one ends up with a classic value of the Strouhal number.

When the tandem type arrangement is embedded within the boundary layer, several features can be pointed out depending on its height and on the upstream or downstream microphone location :

. For the lowest height ($h/\delta_0 = 0.18$), we can estimate that the manipulator wake is about to reach the upstream microphone lcoation. An important decrease is observed on the spectrum in almost all the explored frequency range. It also appears that a "smooth" bump exists close to 6.5 KHz. However, at $Xd/\delta_0 = 5.5$, one can note a small increase for low frequencies, less than 2 KHz, and then the spectrum goes back to the "undisturbed" state.

. For $h/\delta_0 = 0.35$ and 0.71, the $\overline{p'^2}$-spectra exhibit the same tendancy at $Xd/\delta_0 = 0.8$: there is a decrease in pressure density for the relatively low frequencies up to 3 KHz. At $Xd/\delta_0 = 0.55$, the deficit still exists for $h/\delta_0 = 0.71$ but is a little bit weaker at the very low frequencies and spreads up to 4 KHz. Nevertheless, for $h/\delta_0 = 0.35$, the pressure spectrum exhibits almost the same behaviour as the one recorded for $h/\delta_0 = 0.18$ and $Xd/\delta_0 = 0.80$; a "smooth" bump still exists at about the same frequency. In that specific case, one can also guess that the manipulator wake has reached the microphone location.

Thus, this spectral analysis has revealed that the modification on the pressure spectrum was strongly dependant upon the manipulator position within the turbulent boundary layer and upon the streamwise abscissa downstream of the tamdem devices. Anyway, a maximum decrease of - 2 or - 3 dB has been observed in the low frequency range, let say up to 2 KHz, just behind the manipulator ; that leads to a reduction in the pressure fluctuations (and not energy) of approximately 11 - 16%.

Conclusion

This experimental study has shown that similarities exist between either thin or aerofoil section devices in the way that they can produce more or less large skin-friction reductions downstream the manipulator. However, working with aerofoil-shaped devices, no nett drag reduction was recorded because of the manipulator drag penalty and of the short available manipulated length. Looking back to results published in literature one could believe that with greater streamwise distances, it be possible to achieve positive drag reduction.

Numerous hot-wire measurements behind a tandem type configuration have revealed that the manipulator wake plays an important part in the dynamics of the flow. This wake interacts with the large scale motion of the pre-existing undisturbed turbulence and modifies it. Consequently, this interaction leads to the damping of the large scale structure and the production of new energetic small scales ; important decreases on the three components of the Reynolds stress tensor have been recorded. Furthermore, spectral analysis pointed out the possibility to get reduced pressure fluctuations downstream such external manipulators.

As these areofoil-shaped devices work well in terms of skin-friction reduction, the next step in the way to flight applications is to experiment such devices at higher chord Reynolds numbers. The study of the effect of such manipulators on slender bodies might be undertaken, at ONERA, for values of the Reynolds number larger than those considered in the reported experimental work.

Applying turbulence models to manipulated flows is also part of the research which is going on at ONERA/CERT[23],[24]. When looking to manipulator geometry optimization, results obtained so far are in good agreement with the experimental ones ; thus, the numerical code could be used to access the performance of these external manipulators.

IV. Internal manipulators

The growing insight into the processes which alter the turbulence in a boundary layer over a surface leads to the conviction that it must be possible to modify it by changing the surface geometry. That deals with the second passive approach which involves small streamwise surface grooves the dimensions of which are usually scaled in wall variables ; these grooved surfaces are commonly called : "riblets".

A lot of research has been undertaken at NASA Langley[2],[4],[25],[26] and other institutions ([27],[28],[29],[30] for instance) ; in these investigations, straight ribs oriented in the streamwise direction have been used successfully to reduce the turbulent wall shear stress. The best of the 2D "riblet" surfaces produces about 8% nett drag reduction. First results published in the Soviet literature[31] showed that the reduction in turbulent friction obtainable using longitudinal ribbing can amount to 8 - 10%. Let us point out that research is, so far, carried out at I.M.S.T.[32] concerning the effect of small

striations on laminar boundary layers : results showed that the shear stress is increased over a peak and decreased in the valley, and that the transverse component of the velocity is negligible. However, according to the authors, more detailed experiments are necessary in order to check if there is any drag change.

The results of all these studies would be useful not only for engineering applications but also for competitive sports. Indeed, it was just a year ago or so that we learned the news that "Stars and Stripes" had used "riblet" material on the hull and keel in the final rounds of her successful campain to win the America's cup. This example clearly shows up the growing interest for studying the modification to the flow brought with small streamwise ribs.

We will, at first, present data which is representative of the large scale motion and the changes they undergo with such internal manipulators : results of test of five "riblet" models are compared with those obtained for a smooth surface. Then, we will address the question of what mechanisms are responsible for this reduced skin-friction process and what alterations of the turbulent boundary layer they lead to. For that, we will briefly resum results given by some spectral analysis.

Performances of such internal manipulators

The used "riblet" models allow to check the effect of rib spacing (s), rib height (h) and transverse cross-section shape. Furthermore, the influence of yaw angle has also been considered ; in that case, the grooves are aligned at a given angle, ϕ , to the direction of the mean external 2D flow.

For a given model geometry, that is to say for fixed values of s and h, variations of the free-stream velocity (14-38 ms^{-1}) provide variations of the s^+,h^+ paramaters. The height and spacing have been scaled with the inner (or wall) variables of the turbulent boundary layer, i.e. the kinematic viscosity, ν , and the friction velocity, u_τ ($u_\tau = ue\sqrt{Cf/2}$ where ue denotes the streamwise velocity at the outer edge of the boundary layer): $h^+ = h\,U_\tau/\nu$ and $s^+ = s\,U_\tau/\nu$.

The performances of these internal manipulators have been judged through variations of the drag coefficient ; these latter are estimated from the differences between momentum thicknesses, θ , evaluated just behind the "riblet" surface, the length of which is L (fig.12). Then, the estimation of the decrease (or increase) of viscous drag coefficient is given through the formula :

$$\left.\frac{\Delta Cd}{Cd}\right|_{\text{over L}} = \frac{\theta_1 \text{"riblet"} - \theta_1 \text{ smooth}}{(\theta_1 - \theta_0)\text{ smooth}} = \frac{\Delta\theta_1}{\Delta\theta}$$

The value of the momentum thickness, taken at station 1, is obtained through hot-wire surveys. Because of the difficulty for measuring small variations in θ , behind grooved surfaces, about forty to fifty surveys have been performed covering the entire free-stream range for each model. We will only present the averaged value, explaining, then the rather smooth evolution of the curve $\Delta Cd/Cd$ when plotted versus U_∞ , h^+ or s^+.

At last, let us mention that the two possible arrangements described in paragraph II (Internal manipulator : configurations B and T) give practically the same evolution for the variation of the drag coefficient when the manipulated length of the boundary layer is equal to 0.64 m [6]. That means that the parasitic drag due to the facing step (located upstream or downstream depending on the configuration) does not play a determinant role. Anyway, all the results described below have been obtained with configuration T : the tops of the grooves are aligned flush with the adjacent smooth walls.

Drag measurements results :

A synthesis of experimental results is presented on figure 13 for the three-machined aluminium models. The ranges of explored h^+ and s^+ are : h^+ : 8 - 23, s^+ : 8 - 52. Data from the different models collapse better when plotted versus h^+ rather than s^+ ; h^+ appears to be the "crucial" parameter. For the three models, with different aspect ratio s/h, nett reductions are achieved when $h^+ < 13$ though s^+ can reach several tens of wall units. Maximum decreases of 10 - 15% are recorded for h^+ less to 10. One has to be aware that the amount of nett drag reduction might be subject to discussions since the formula, we used to get it, is very sensitive to a lot of parameters. Anyway, it is in terms of "tendancy" that we have to interpret the results. For $h^+ < 13$, nett drag reductions could be achieved though increases are recorded when h^+ is greater than 18 for any of the three models.

Though there is no drag penalty involved with such devices, we can nevertheless observe that the larger the ratio s/h is (2 or 3), the greater the amount of drag reduction appears to be. Let us recall that the increase of wetted area is smaller when this ratio s/h is greater. Furthermore, results from figure 13 suggest that increasing the aspect ratio s/h may have the effect of reducing the upper limit of h^+ for which $\Delta Cd/Cd$ is less than zero or extending the upper limit of s^+ for which drag reductions have been recorded.

Figure 14 presents data for vinyl riblet model s = h = 0.152 mm, obtained from the 3M Company. The variations of the free-stream velocity allow us to cover the range : h^+ : 5.5 - 14.5. Whatever the value of h^+ is, reductions of the viscous drag coefficient over 0.64 m of "riblet" model length have been recorded [33], with a maximum of reduction close to 7 - 8 in terms of wall units. Below that value, one can guess that the variation of the viscous drag coefficient will go back slowly to some limit the value of which is not really known ; indeed, for a given aspect ratio s/h, $h^+ = 0$ does not correspond exactly to the smooth or reference case. On that same figure, we have reported data obtained from the machined aluminium model with the same aspect ratio, s/h. By extrapolating the vinyl-model curve, it appears that this curve will intersect the axis $\Delta Cd/Cd = 0$ at about the same h^+ value as the aluminium-model curve. However, the level of drag reduction is not identical though the technique used to evaluate it did not change. Although the two "riblets" provide with the same increase of wetted area and have the same supposed triangular V-shape, their cross-section might be different in some way. Let us mention that enlargements have revealed that the ribs were not uniform in the transverse direction

for the machined model ; this observation could not be made for the 3M vinyl one.

Influence of curvature :

Figure 15 shows up drag data for the vinyl riblet model s # 3.5 h = 0.46 mm in the same type of diagram. Results are compared to those provided with the symmetric V-shaped machined aluminium model s = 3h = 0.6 mm which has approximately the same aspect ratio s/h.

Only couple of percents of nett drag reduction have been recorded (2 - 4%) ; moreover, the upper limite of h^+ giving drag reduction is smaller and close to 6. As the geometry of this model consists of grooves with valley and peak curvatures, this result shows that curvature has negative effect on drag reduction performance. That is consistent with results obtained at NASA Langley by Walsh[25] and Walsh et al.[26]. Unfortunalely, it was not possible to dissociate the influence of peak or valley curvature. Nevertheless, whatever the shape of the valley is, low speed fluid lies there ; one could then believe that increasing the radius of peak curvature makes larger the area exposed to maximum shear stress and, as a consequence, diminishes the possible averaged skin-friction reduction.

Influence of yaw angle :

If one considers the possibility of applying such internal manipulators to aircraft applications, it is very important to look at the sensitivity of grooved surfaces to yaw angles. The ribs are making an angle ϕ with the machined aluminium model : s = 2h = 0.5 mm for ϕ = 10° and 20°. The model length is L = 0.32 m. The variations of the viscous drag coefficient, over the manipulated boundary layer length L, are estimated from the formula given at the beginning of paragraph : Performances of such internal manipulators. Because of the short value of L, which induces a small variation of $\Delta\theta$, one can notice, through that formula, that a small uncertainty on measurements of the momentum thickness θ_1 may produce a rather important variation of the estimation of $\Delta Cd/Cd$. This is the reason why there is some scattering on drag data and why hatching domains are used to report these data.

On figure 16, we have plotted versus u_∞ and/or h^+ the quantity :

$$\left.\frac{\Delta Cd}{Cd}\right|_{\phi \neq 0} \Big/ \left.\frac{\Delta Cd}{Cd}\right|_{\phi = 0}$$

For low values of h^+, to which correspond important drag reductions, this ratio is close to 1 for ϕ = 10° and 20°. When h^+ increases, an angle of 10° yields also to skin friction reductions, over the explored range of h^+, which are weaker than at ϕ = 0°. Anyway, the behaviour of the two curves $\frac{\Delta Cd}{Cd}$ (h^+) is identical for both ϕ = 0° and 10°. On the other hand, for ϕ = 20°, increases on the drag coefficient are recorded while there are still some reductions for 10° and 0°. This expresses that the upper limit of the h^+ domain decreases as the angle of yaw increases. Besides that, the averaged skin-friction reductions are lower than those obtained for ϕ = 10°. Let us mention that this analysis implicitely assumes there is no manipulator imperfection (same cross-section, same V-shaped...) which might not be true.

In a second experiment, we have looked at the effect of an angle of 20° on the 3M-vinyl model : s = h = 0.152 mm ; the manipulated length is in that case equal to 0.64 m. Results are plotted on figure 17 in a $\Delta Cd/Cd - h^+$ representation. Same conclusions can be drawn for that model as for the preceding one : nett drag reductions still exist but are weaker in a shorter h^+-range.

This study shows up that "riblets" keep a beneficial effect for angles of yaw up to 20°. These results are consistent with those obtained by Walsh et al[26] for ϕ = 15° and 30° : they obtained smaller reductions at ϕ = 15° and drag increases at ϕ = 30° for the considered range of s^+ : 10 - 50.

Turbulence data

Measurements have been performed very close to the trailing edge of the "riblet" model and upon the model in order to look at the response of the boundary layer to such an internal manipulation.

Components of the Reynolds Stress Tensor :

The five components of the Reynolds tensor have been determined using a miniature X-wire probe just behind the following "riblet" geometry : s = 2h = 0.5 mm, L = 0.64 m. The external free-stream velocity is close to 16 ms^{-1} ; in that case the nett drag reduction recorded is about 6 - 7%. The traverse location is at about 1 000 wall units from the "riblet" trailing edge. Results for $\overline{u'^2}$, $\overline{v'^2}$ and $\overline{u'v'}$ are given on figure 18. The surveys reveal there is no modification on the turbulent profiles, at least in the outer part of the boundary layer ; unfortunately, the size of the probe did not allow to go closer to the wall, below y^+ = 20.

Spectral analysis :

This analysis has been developed using the same technique as the one described in paragraph III (- Spectral analysis). In order to approach the structure of the flow in the viscous sub-layer, it is necessary to deal with a straight-wire probe ; we consider a classic DISA 55 P 15 ; the characteristics of the wire are : length : 1.25 mm, diameter : 5 µm. Spectra of the streamwise fluctuation intensity, $\overline{u'^2}$, will only be presented.

. Such an analysis has been at first performed just downstream of the "riblet" model : s = 3h = 0.6 mm, L = 0.64 m. The external free-stream velocity is close to 16 ms^{-1}, which corresponds to h^+ # 8. Figure 19 shows the streamwise velocity spectra for two heights within the turbulent boundary layer : y^+ = 21 and 210. The results are reported in a k E(k)-representation where E denotes the normalized energy density associated with the wave number k. There is no apparent difference on the $\overline{u'^2}$-spectra behind smooth or ribbed plates, set according to configuration B or T, see paragraphe II (- Internal manipulators). As the integral of this spectrum provides with the r.m.s. value, this result confirm that there is no modification on the streamwise component of the Reynolds Stress Tensor.

. $\overline{u'^2}$-spectra have then been performed upon the vinyl model s = h = 0.152 mm, L = 0.64 m at the streamwise abscissa x = 0.75 L downstream of the leading edge of the "riblet". The free-stream velocity is close to 16 ms^{-1} , which provides with $h^+ \# 6.5$. Figure 20 reports the streamwise fluctuations spectra for four positions lying either in the viscous sub-layer or buffer layer : $y^+ = 4.3$, 6.4, 12.8 and 21.4. Results are compared to the smooth plate case. For $y^+ = 4.3$, one can notice that the energy level is weaker for the high frequency range and stronger in the low frequencies, above the ribbed plate. However, by moving away from the wall, the energetic transfert is inverted. Indeed, at $y^+ = 21.4$, the energy is more important for the high wave numbers and, less important for the low wave numbers.

Let us recall that the spectral analysis allows to precise the structure of a turbulent flow from either an energy purpose or a dimensional one (small or large structures). Thus, we can get information about the energy distribution depending on wave number or frequency, to which correspond length scale or time scale. Then, from this analysis above the "riblet", one might suggest that the grooves induce a deficit of small scale structures at the upper part of the viscous sublayer while these structures are in excess around the middle of the buffer layer.

So, by changing wall geometry, there is a redistribution of energy within the internal part of the boundary layer where, according to several investigators, 70% of the total production of turbulence occurs.

Anyway, if one wants to look precisely at the possible alterations of the dissipative structures, which are in excess in the internal region, one has to be aware that the probe size is maybe too important versus the length scale of these structures. That means that such a spectral analysis must be considered as a qualitative even comparative (smooth-ribbed surface) approach and analyzed in such a way.

Pressure fluctuations :
Same microphones, as the ones described in section "Spectral Analysis", paragraph III, have been mounted downstream the "riblet" model : s # 3.5 h = 0.46 mm at a given external velocity corresponding to $h^+ \# 5.5$. Whatever the location of the microphone is, there is no perturbation on the p'^2-spectra on the explored frequency range : 32 Hz - 25 KHz. Furthermore, by considering a combination of the two passive approaches (tandem aerofoil-shaped devices + "riblet" model), the disturbed p'^2-spectrum is quite identical to the one obtained by manipulating the boundary layer with only external manipulators.

Conclusions

In zero pressure gradient flows, several features could be pointed out as regards to the manipulation of turbulent boundary layers through internal manipulators :

- When the "riblet" geometry is reduced in size to less than 13 wall units in height and couple of tens wall units in the transverse direction, nett drag reductions are achieved. The amount of drag seems to be dependant on the increase of wetted area ; moreover, peak curvature has negative effect on such manipulators performance.

- Spectral measurements of streamwise turbulence intensity fluctuations and wall pressure fluctuations have been performed just downstream of the streamwise grooves : no apparent modification compared to the smooth wall case was recorded. However, u'^2-spectra obtained upon the "riblet" have shown that some energy re-distribution may exist within the internal part of the boundary layer. These measurements might suggest that, close to the wall, these small striations would induce more confined small structures than on the smooth plate.

- The sensitivity of grooved surfaces to yaw angles has been checked. It reveals that "riblets" keep a beneficial effect for angles of yaw up to 20° ; nett drag reductions are still recorded but are weaker.

These "fundamental" experiments, undertaken in a low-speed wind-tunnel have allowed to verify, with laboratory measurements, that some "riblet" models could provide us with turbulent skin-friction reductions, for 2D boundary layers developing in zero-pressure gradient flows. The next step was to go closer to flight applications and to look at the effect of small streamwise grooves on a slender body in a subsonic wind-tunnel and on a cylindrical body in a transonic wind-tunnel. These experiments have been very positive in the sense that they led to nett skin-friction drag reductions (Detailed information can be found in[7] and [34]) and will be pursued at ONERA on a larger fuselage.

Then, of the two methods which have been tried, the case of "riblets" appears to be well proven ; they may have the potential of being an integral-design feature by being moulded into the surface or by replacing a sheet of painting by a thin-vinyl one made of small streamwise grooves.

At last, let us mention that research upon "riblets" also involves a numerical approach. So far, the parabolized Navier-Stokes equations are solved for a laminar flow developing on a ribbed surface. The code will be, then, extended to turbulent flows.

REFERENCES

1. V. Schmitt : 24ème Colloque AAAF (Poitiers, 1987).
2. D.M. Bushnell : AGARD REPORT 723 (1985).
3. A.S.W. Thomas : AGARD REPORT 723 (1985).
4. S.P. Wilkinson ; J.B. Anders ; B.S. Lagos ; D.M. Bushnell : Int. Conf. on Turbulent Drag Reduction by Passive Means (London, 1987).
5. E. Coustols ; J. Cousteix : La Recherche Aérospatiale (English Edition) n° 1986-2.
6. E. Coustols ; J. Cousteix ; J. Belanger : Int. Conf. on Turbulent Drag Reduction by Passive Means, (London, 1987).
7. E. Coustols ; C. Gleyzes ; V. Schmitt ; P. Berrué: 24ème Colloque AAAF, (Poitiers, 1987).
8. G. Pailhas ; J. Cousteix : La Recherche Aérospatiale (English Edition) n° 1986-2.
9. J.N. Hefner ; J.B. Anders ; D.M. Bushnell : AIAA Paper n° 83-0293 (1983).

10. J.B. Anders ; J.N. Hefner ; D.M. Bushnell : AIAA Paper n° 84-0345 (1984).
11. J.B. Anders ; R.D. Watson : AIAA Paper n° 85-0520 (1985).
12. A. Bertelrud ; T.V. Truong ; F. Avellan : AIAA Paper n° 82-1370 (1982).
13. L.W. Reidy ; T.S. Mautner : NAOSC TH 1445.
14. R.E. Falco ; N. Rashidnia : Int. Conf. on Turbulent Drag Reduction by Passive Means (London, 1987)
15. J.B. Anders : SAE Technical Papers Series n° 86-1769 (1986).
16. R. Houdeville ; J.C. Juillen ; J. Cousteix : La Recherche Aérospatiale (English Edition) n° 1984-1.
17. V.D. Nguyen ; J. Dickinson ; J. Lemay ; D. Provencal ; Y. Jean ; Y. Chalifour : 14th Congress ICAS (Toulouse, 1984).
18. J. Lemay ; A.M. Savill ; J.P. Bonnet ; J. Delville : Sixth Symposium on Turbulent Shear Flows (Toulouse, 1987).
19. Y.G. Guezennec ; H.M. Nagib : AIAA Paper n° 85-0519 (1985).
20. G. Pailhas : Rapport Technique CERT/DERAT (1986).
21. A.M. Savill : IUTAM Symposium on Turbulent Management and Relaminarization (Bengalore, 1987).
22. J. Evrard : Ph. Dissertation (in preparation).
23. E. Coustols ; C. Tenaud ; J. Cousteix : Sixth Symposium on Turbulent Shear Flows (1987).
24. C. Tenaud ; E. Coustols ; J. Cousteix : Int. Conf. on Turbulent Drag Reduction by Passive Means (London, 1987).
25. M.J. Walsh : AIAA Paper n° 82-0169 (1982).
26. M.J. Walsh ; A.M. Lindemam : AIAA Paper n° 84-0347, (1984).
27. D.W. Bechert ; G. Hoppe ; W.E. Reif : AIAA Paper n° 85-0546 (1985).
28. J.A. Gallagher ; A.S.W. Thomas : AIAA Paper n° 84-2185 (1984).
29. W.G. Sawyer ; K.G. Winter ; Int. Conf. on Turbulent Drag Reduction by Passive Means (London, 1987).
30. K.S. Choi ; H.H. Pearcey ; A.M. Savill : Int. Conf. on Turbulent Drag Reduction by Passive Means (London, 1987).
31. G.V. Enyutin ; Yu. A. Lashkov ; N.L. Samoilova ; I.V. Fadeev ; E.A. Shumilkina : Translated from Izvestiya Akademii Nauk SSSR (March-April, 1987).
32. L. Fulachier ; L. Djenidi ; F. Anselmet : 24ème Colloque AAAF (Poitiers, 1987).
33. F. Fioc : Ph. D. Dissertation (in preparation).
34. E. Coustols ; A. Seraudie ; A. Mignosi : J.F. Breil : Rapport Technique CERT/DERAT (1988).

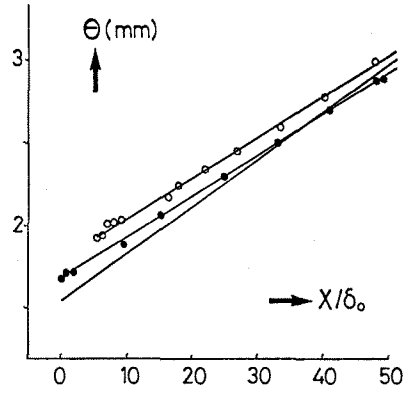

Fig. 1 : Streamwise evolutions of θ — without device • single device c/δ_o = 0,75, t/δ_o = 0.007, h/δ_o = 0,3 o tandem device c/δ_o = 1.2, t/δ_o = 0.007, h/δ_o = 0.35, s/δ_o = 6

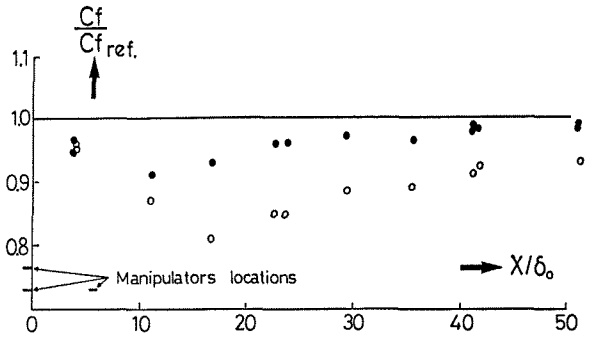

Fig. 2 : Streamwise evolution of C_f (same symbols as Fig. 1).

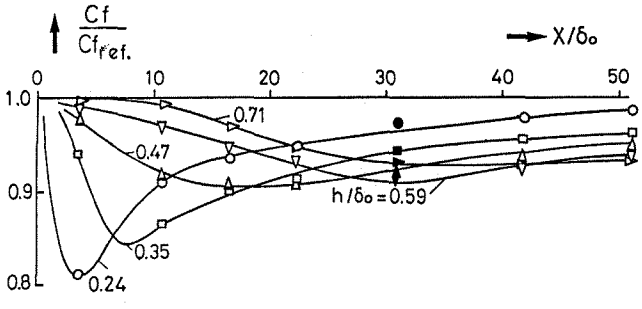

Fig. 3 : Streamwise evolution of C_f - single NACA 0009 device (open symbols : hot-element gauge ; filled symbols : drag balance).

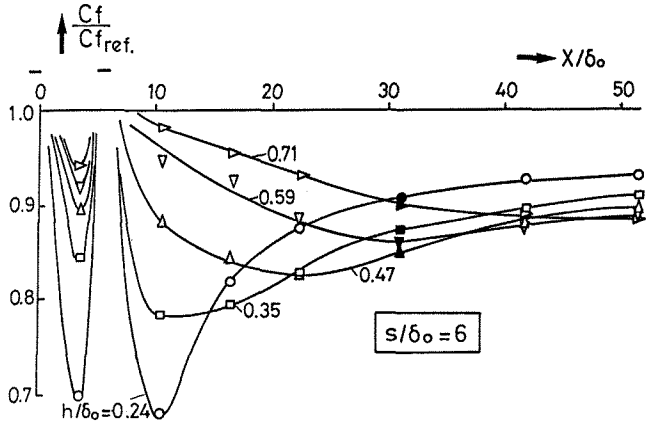

Fig. 4 : Streamwise evolution of C_f - tandem NACA 0009 devices (same symbols as in Fig. 3).

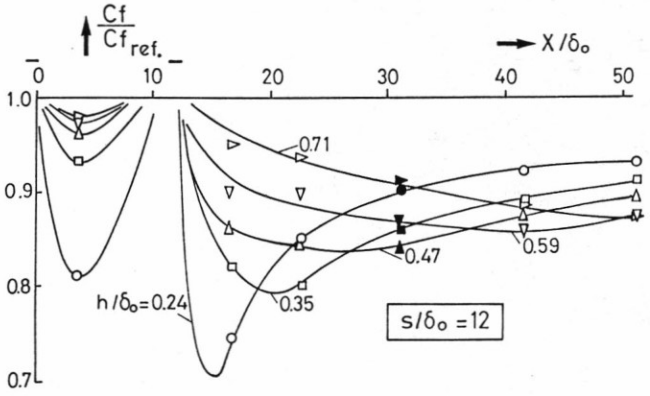

Fig. 5 : Streamwise evolution of Cf - single NACA 0009 device. (open symbols : hot-element gauge ; filled symbols : drag balance).

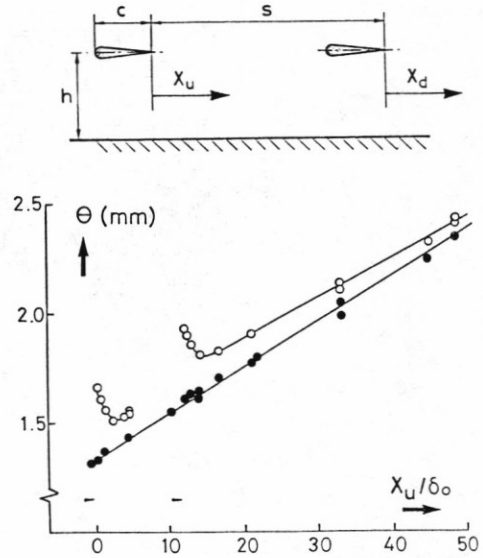

Fig. 6 : Streamwise evolution of θ • without manipulator, o with tandem NACA 0009 devices $c/\delta_o = 1.2$ $h/\delta_o = 0.3$ $s/\delta_o = 12$.

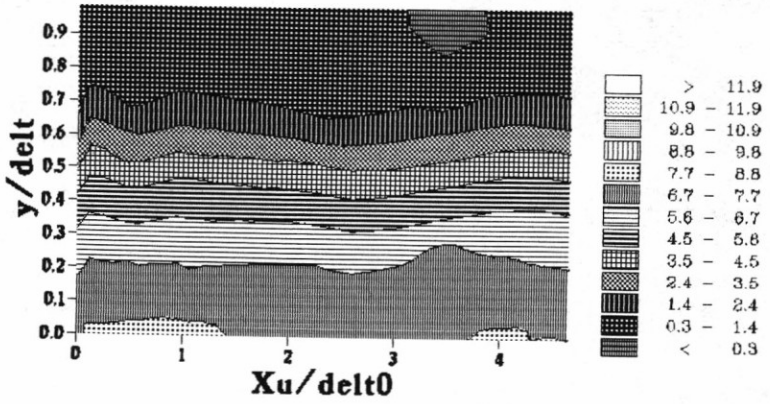

Fig 7a : Iso-streamwise velocity fluctuations $(10^2 \ (\overline{u'^2})^{1/2} \ / \ Ue)$ without manipulator.

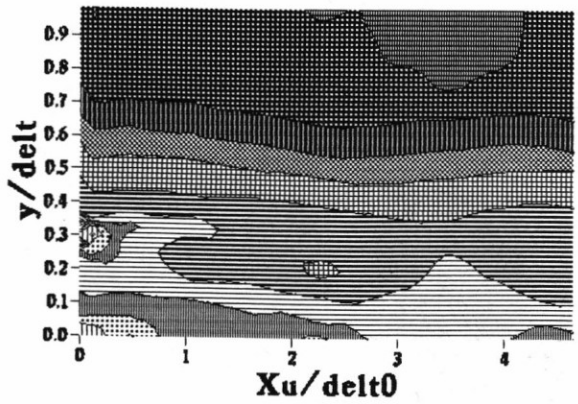

Fig. 7b : Cont. downstream the upstream device (same patterns scale as Fig. 7a).

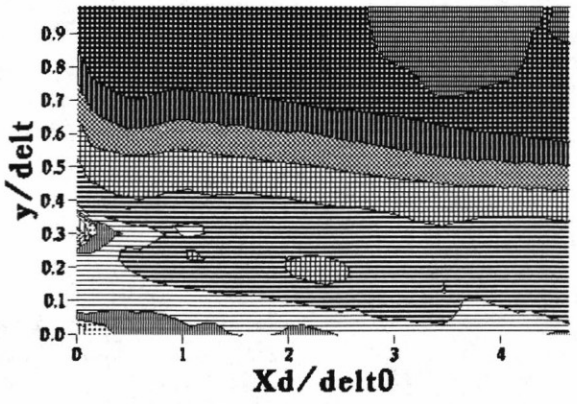

Fig. 7c : Cont. downstream the downstream device (same patterns scale as Fig. 7a).

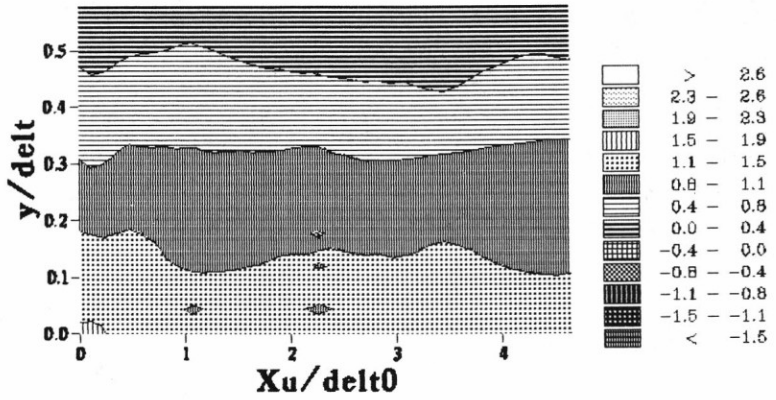

Fig. 8a : Iso-shear stress contours (-10^3 $\overline{u'v'}/Ue^2$) without manipulator.

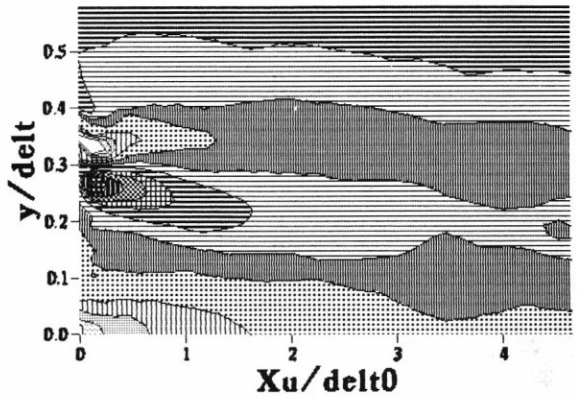

Fig. 8b : Cont. - downstream the upstream device (same patterns scale as Fig. 8a).

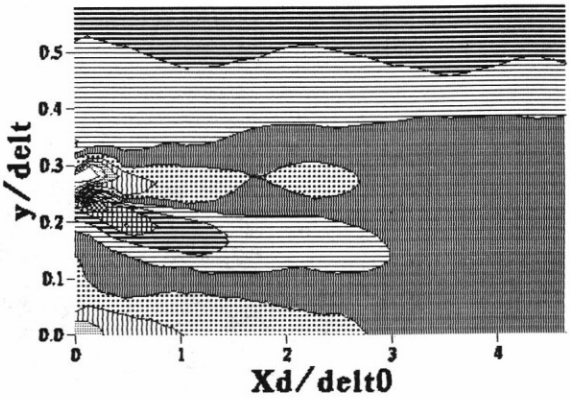

Fig. 8c : Cont. - downstream the downstream device (same patterns scale as Fig. 8a).

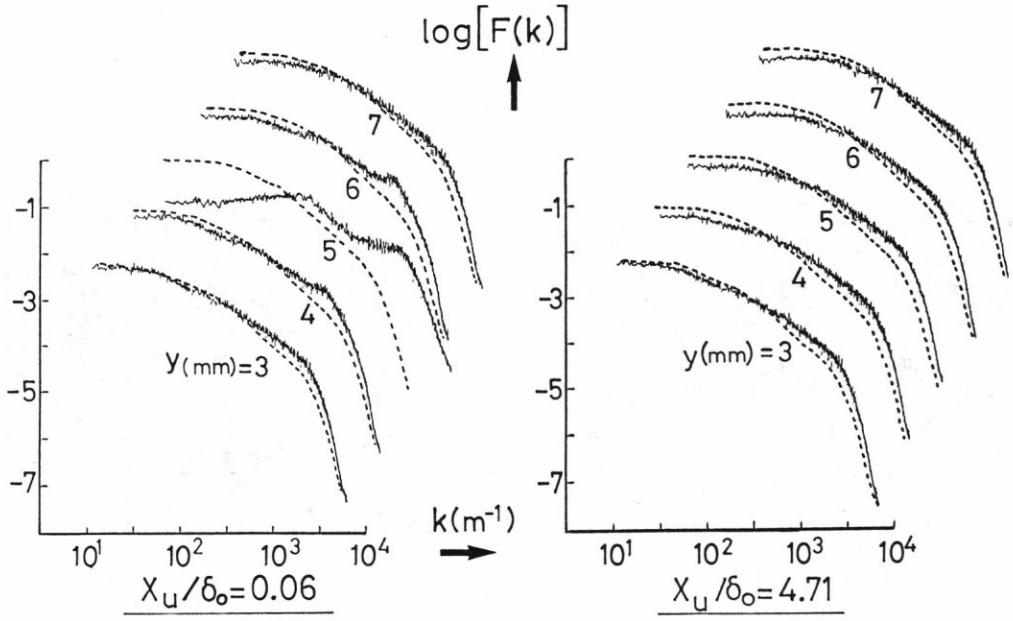

Fig. 9 : Streamwise fluctuations spectra (----- without manipulator).

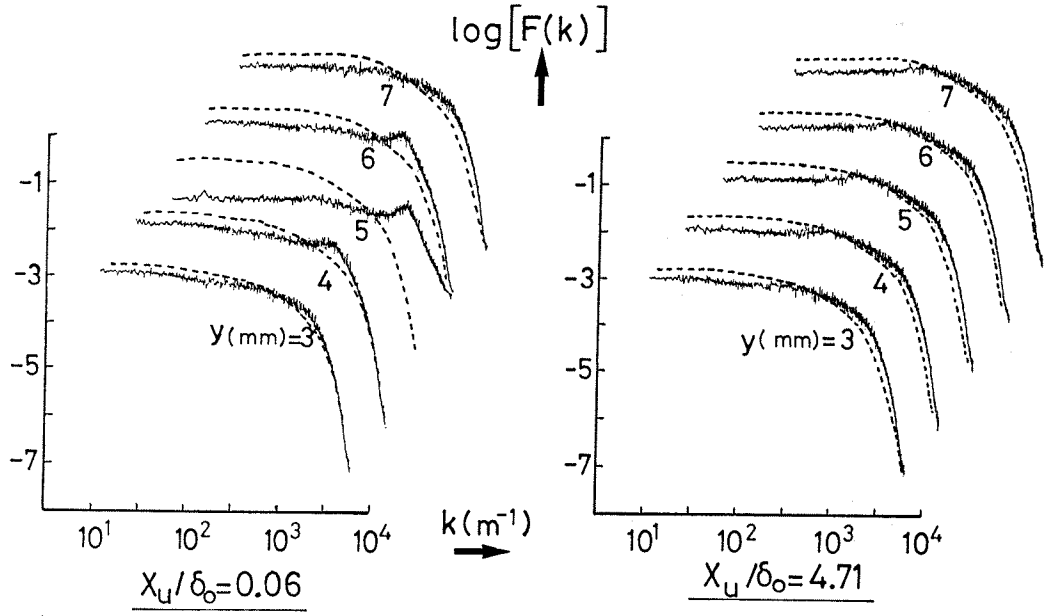

Fig. 10 : Normal to the wall fluctuations spectra (------ without manipulator)

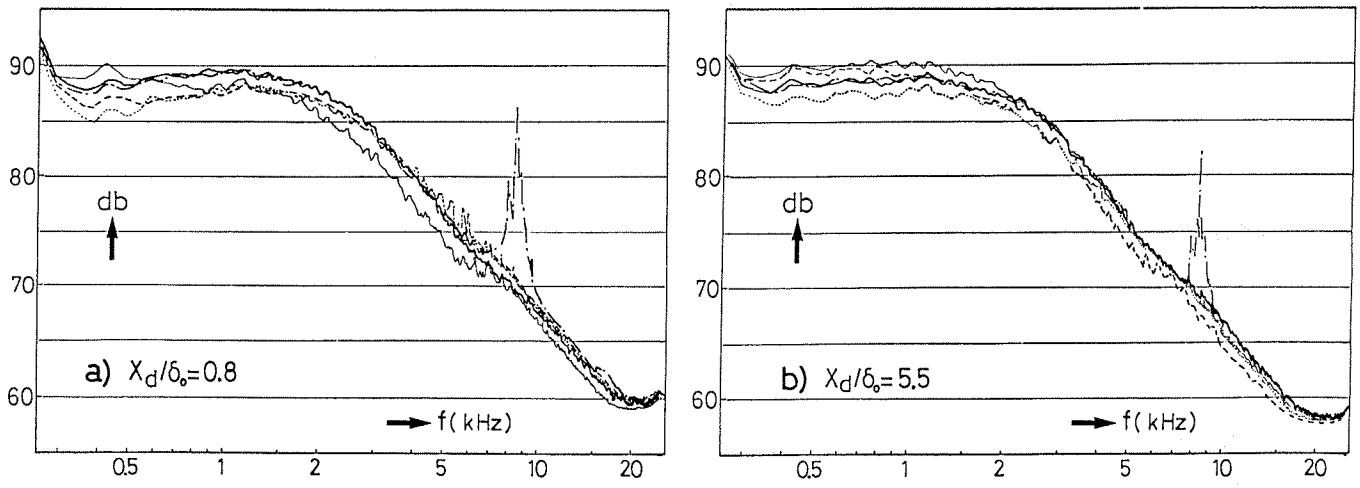

Fig. 11 : Pressure fluctuations spectra (—— without manipulator, — .— h/δ_o = 1.5, ... h/δ_o = 0.71, ---- h/δ_o = 0.35, —— h/δ_o = 0.18).

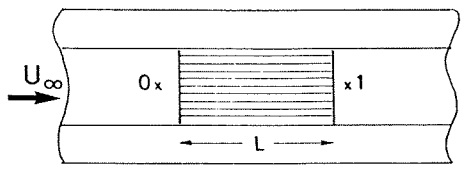

Fig. 12 : Experimental set-up (viewed from above).

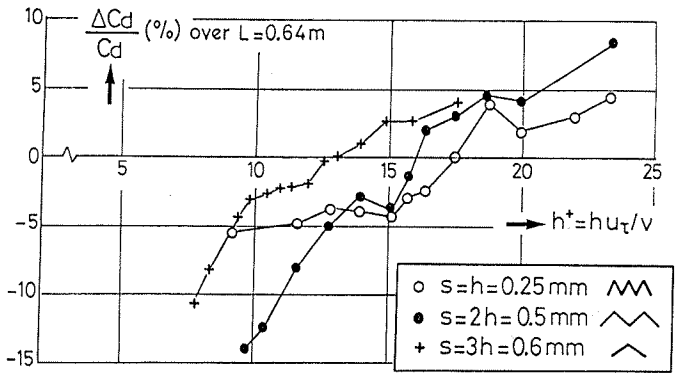

Fig. 13 : Synthesis of drag data for machined aluminium models.

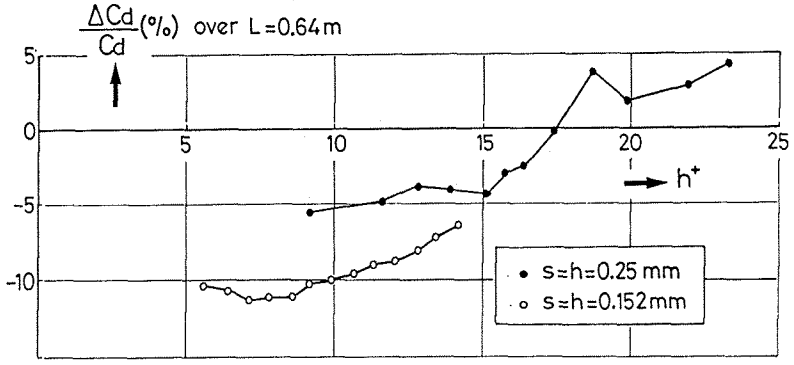

FIG. 14 : Drag data for two "riblet" models (o vinyl, • aluminium).

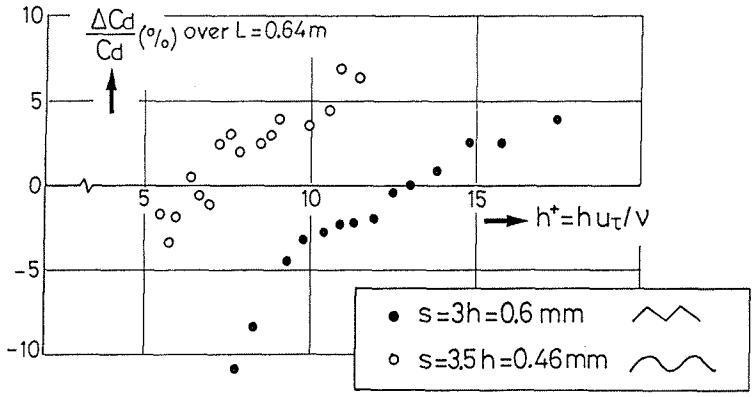

Fig. 15 : Influence of peak and valley curvature.

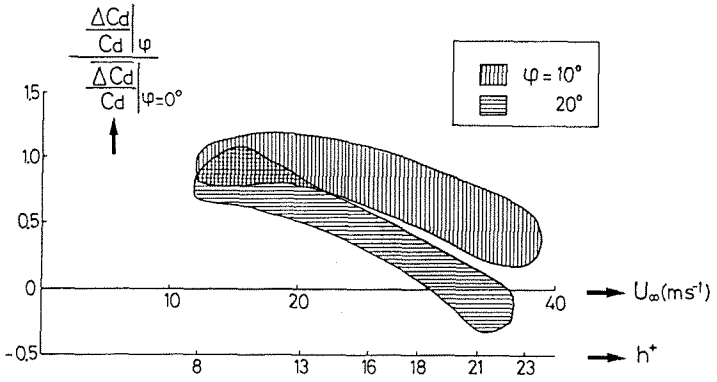

Fig. 16 : Influence of yaw angle ($s = 2h = 0.5$ mm - $L = 0.32$ m).

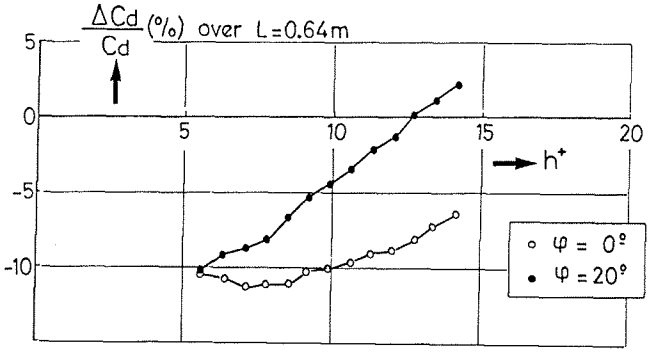

Fig. 17 : Influence of yaw angle
($s = h = 0.152$ mm - $L = 0.64$ m).

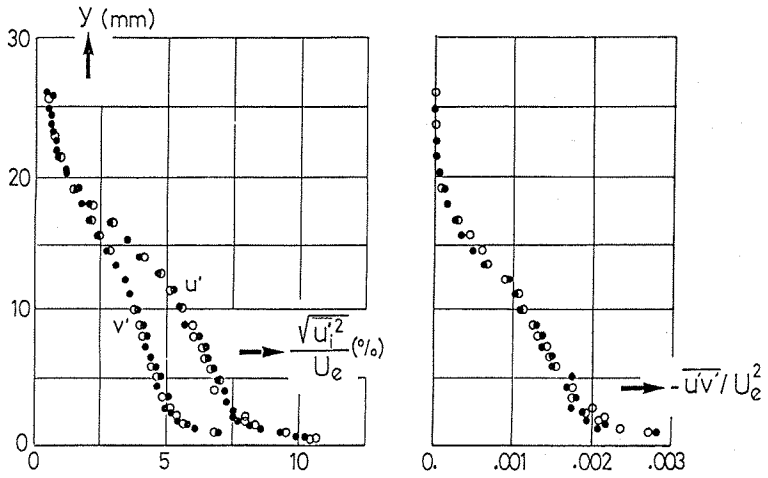

Fig. 18 : Reynolds stress components just behind the ribbed plate (● smooth wall, o "riblet" s = 2h = 0.5 mm - L = 0.64 m).

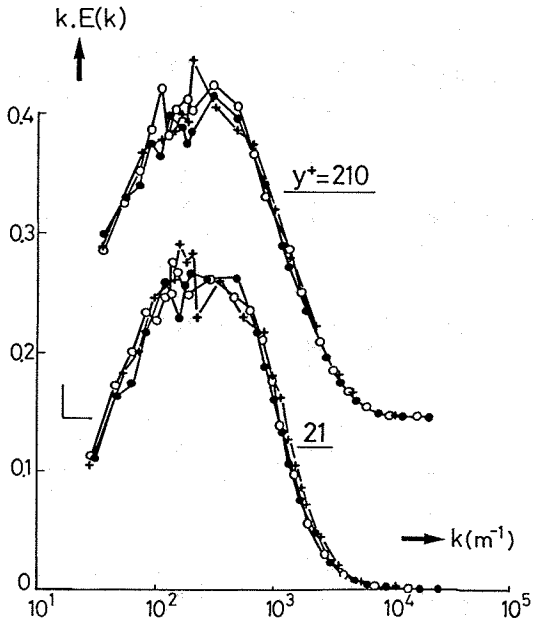

Fig. 19 : $\overline{u'^2}$ spectra behind the ribbed plate s = 3h = 0.6 mm - L = 0.64 m (+ smooth wall, o "riblet"- conf. B, ● "riblet"- conf. T).

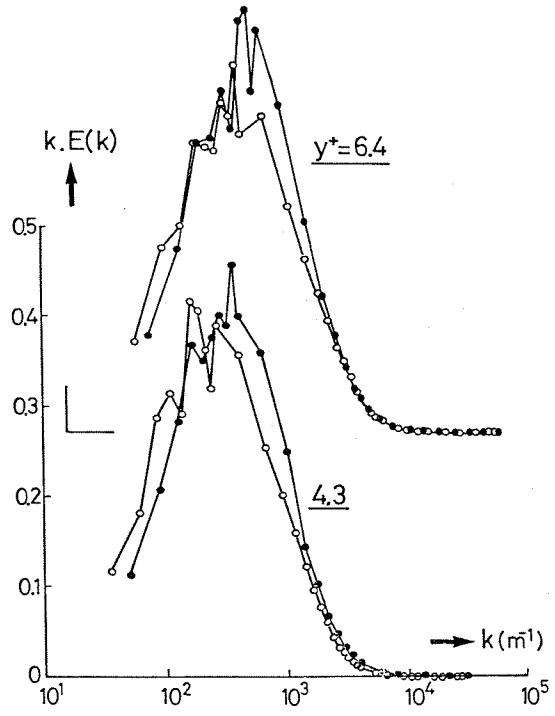

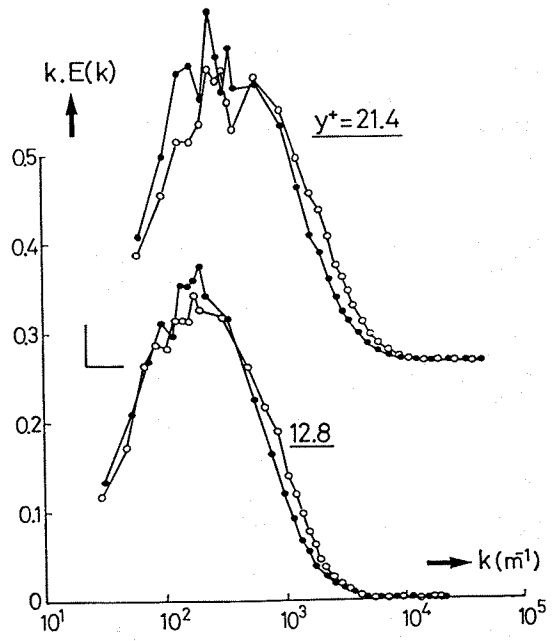

Fig. 20 : $\overline{u'^2}$ - spectra upon "riblet" s = h = 0.152 mm (● smooth wall, o "riblet").